doi:10.1093/brain/awz287 BRAIN 2019: 142; 3440–3455 | 3440

BRAIN
A JOURNAL OF NEUROLOGY

A quantitative neuropathological assessment of translocator protein expression in multiple sclerosis

Erik Nutma,[1] Jodie A. Stephenson,[1,2] Rianne P. Gorter,[1] Joy de Bruin,[1] Deirdre M. Boucherie,[1] Cornelius K. Donat,[3] Marjolein Breur,[1] Paul van der Valk,[1] Paul M. Matthews,[3,4] David R. Owen[3] and Sandra Amor[1,2]

The 18 kDa translocator protein (TSPO) is increasingly used to study brain and spinal cord inflammation in degenerative diseases of the CNS such as multiple sclerosis. The enhanced TSPO PET signal that arises during disease is widely considered to reflect activated pathogenic microglia, although quantitative neuropathological data to support this interpretation have not been available. With the increasing interest in the role of chronic microglial activation in multiple sclerosis, characterising the cellular neuropathology associated with TSPO expression is of clear importance for understanding the cellular and pathological processes on which TSPO PET imaging is reporting. Here we have studied the cellular expression of TSPO and specific binding of two TSPO targeting radioligands (^{3}H-PK11195 and ^{3}H-PBR28) in tissue sections from 42 multiple sclerosis cases and 12 age-matched controls. Markers of homeostatic and reactive microglia, astrocytes, and lymphocytes were used to investigate the phenotypes of cells expressing TSPO. There was an approximate 20-fold increase in cells double positive for TSPO and HLA-DR in active lesions and in the rim of chronic active lesion, relative to normal appearing white matter. TSPO was uniformly expressed across myeloid cells irrespective of their phenotype, rather than being preferentially associated with pro-inflammatory microglia or macrophages. TSPO+ astrocytes were increased up to 7-fold compared to normal-appearing white matter across all lesion subtypes and accounted for 25% of the TSPO+ cells in these lesions. To relate TSPO protein expression to ligand binding, specific binding of the TSPO ligands ^{3}H-PK11195 and ^{3}H-PBR28 was determined in the same lesions. TSPO radioligand binding was increased up to seven times for ^{3}H-PBR28 and up to two times for ^{3}H-PK11195 in active lesions and the centre of chronic active lesions and a strong correlation was found between the radioligand binding signal for both tracers and the number of TSPO+ cells across all of the tissues examined. In summary, in multiple sclerosis, TSPO expression arises from microglia of different phenotypes, rather than being restricted to microglia which express classical pro-inflammatory markers. While the majority of cells expressing TSPO in active lesions or chronic active rims are microglia/macrophages, our findings also emphasize the significant contribution of activated astrocytes, as well as smaller contributions from endothelial cells. These observations establish a quantitative framework for interpretation of TSPO in multiple sclerosis and highlight the need for neuropathological characterization of TSPO expression for the interpretation of TSPO PET in other neurodegenerative disorders.

1 Department of Pathology, Amsterdam UMC, Location VUmc, The Netherlands
2 Centre for Neuroscience and Trauma, Blizard Institute, Barts and the London School of Medicine and Dentistry, Queen Mary University of London, UK
3 Department of Brain Sciences, Imperial College London, UK
4 UK Dementia Research Institute, Imperial College London, UK

Correspondence to: Professor Sandra Amor
Department of Pathology
Amsterdam UMC, location VUmc
1081 HV Amsterdam, the Netherlands
E-mail: s.amor@amsterdamumc.nl

Received February 7, 2019. Revised June 11, 2019. Accepted July 25, 2019. Advance Access publication October 3, 2019

Keywords: translocator protein; multiple sclerosis; microglia; astrocytes; positron emission tomography

Abbreviations: HLA = human leukocyte antigen; NAGM = normal appearing grey matter; NAWM = normal appearing white matter

Introduction

The 18 kDa translocator protein (TSPO) is an outer mitochondrial membrane protein that has attracted increasing interest for its use as a PET imaging target to visualize inflammation in the brain. TSPO is expressed in many tissues, including the brain, and has been suggested to be involved in mitochondrial 'household' functions, although its exact functions are unknown (Vowinckel *et al.*, 1997; Versijpt *et al.*, 2005; Oh *et al.*, 2011; Rissanen *et al.*, 2014; Datta *et al.*, 2017*b*). TSPO PET signal is markedly upregulated in neurodegenerative and neuroinflammatory diseases including multiple sclerosis (Vowinckel *et al.*, 1997; Versijpt *et al.*, 2005; Oh *et al.*, 2011; Rissanen *et al.*, 2014; Datta *et al.*, 2017*b*), Alzheimer's disease (Edison *et al.*, 2008; Yasuno *et al.*, 2008), Parkinson's disease (Ouchi *et al.*, 2005), viral encephalitis (Banati *et al.*, 1999; Cagnin *et al.*, 2001), amyotrophic lateral sclerosis (Turner *et al.*, 2004*a*), Huntington's disease (Meßmer and Reynolds, 1998) and frontotemporal dementia (Cagnin *et al.*, 2004) and thus has become recognized as a marker of *in vivo* neuroinflammation (Banati *et al.*, 2000; Venneti *et al.*, 2006; Colasanti *et al.*, 2014). A limitation of these applications has been uncertainty regarding the interpretation of increased signal; many of the studies have widely assumed that increased signal reflects activated microglia, while ignoring the potential contributions of astrocytes and other cell types (Groom *et al.*, 1995; Vowinckel *et al.*, 1997; Banati *et al.*, 2000; Cagnin *et al.*, 2001; Debruyne *et al.*, 2003; Gerhard *et al.*, 2003, 2004, 2006*a*, *b*; Henkel *et al.*, 2004; Turner *et al.*, 2004*b*; Tai *et al.*, 2007; Tomasi *et al.*, 2008; Venneti *et al.*, 2009; Politis *et al.*, 2015; Ghadery *et al.*, 2017; Yankam Njiwa *et al.*, 2017). Although recent studies using animal models of neurodegenerative diseases have shown astrocytic TSPO (Maeda *et al.*, 2007; Rojas *et al.*, 2007; Arlicot *et al.*, 2008; Ji *et al.*, 2008; Mattner *et al.*, 2011; Lavisse *et al.*, 2012*b*; Daugherty *et al.*, 2013; Dickens *et al.*, 2014; Wang *et al.*, 2014; Lavisse *et al.*, 2015; Sérrière *et al.*, 2015; Domene *et al.*, 2016; Israel *et al.*, 2016; Nguyen *et al.*, 2018), only a few have examined astrocytic expression of TSPO in the human CNS (Kaunzner *et al.*, 2019), and these descriptions have been qualitative rather than quantitative (Cosenza-Nashat *et al.*, 2009; Maeda *et al.*, 2011; Liu *et al.*, 2015).

In experimental autoimmune encephalomyelitis and in cuprizone, two animal models of multiple sclerosis, increased TSPO expression has been described in astrocytes and microglia (Daugherty *et al.*, 2013; Nack *et al.*, 2019). Increased microglial TSPO expression is associated with pro-inflammatory markers in rodents (Beckers *et al.*, 2018). Based on animal model studies, TSPO has been suggested as a therapeutic target for modulation of the pathogenic microglial phenotypes (Daugherty *et al.*, 2013; Ravikumar *et al.*, 2016). However, in humans, TSPO is not upregulated in either pro-inflammatory macrophages (Narayan *et al.*, 2017) or primary microglia (Owen *et al.*, 2017). These *in vitro* data are consistent with the finding that monocytes isolated from people with multiple sclerosis show lower TSPO expression compared to healthy controls (Harberts *et al.*, 2013). Additionally, microglia/macrophages in multiple sclerosis lesions adopt an intermediate phenotype, and the classical M1 (pro-inflammatory) and M2 (anti-inflammatory) phenotypes probably represent extreme states only found *in vitro* (Peferoen *et al.*, 2015). Thus, in contrast to the pattern of TSPO expression in rodent models, it may not be so specifically associated with pro-inflammatory microglia in multiple sclerosis (Zrzavy *et al.*, 2017). For interpretation of TSPO PET studies of brain inflammation in multiple sclerosis and for exploration of potential therapeutic targeting of TSPO, it is thus crucial to determine whether specific microglial markers are associated with TSPO expression and to what extent these cells contribute to the TSPO PET signal in neuroinflammatory diseases *in vivo*.

Here we have performed a quantitative neuropathological study in a large cohort of multiple sclerosis brain and spinal cord tissues to characterize the cell types and identify the phenotypes of microglia expressing TSPO in lesions in the white and grey matter. We report three important findings. First, we confirm previous data showing that TSPO expression is increased in active and chronic active lesions, and that HLA-DR + microglia are the cell type responsible for the majority of the signal. However, astrocytes expressing TSPO in the centre of chronic active and in inactive lesions also are important contributors to the total number of TSPO + cells. Second, we show that, in humans, TSPO reports on microglia density rather than relative microglial activation and polarization. Finally, we confirm a strong, direct relationship between TSPO expression and TSPO radioligand binding in brain tissue *ex vivo*.

Therefore, we show that while expression of TSPO reflects activated microglia, it is misleading to characterize TSPO as a marker restricted to pro-inflammatory microglia.

Materials and methods

Human brain tissue

Human brain tissue was obtained at autopsy from 42 patients with multiple sclerosis and 12 age-matched cases with no neurological disorders or peripheral inflammation. Biopsy material from MRI tumour-like lesions was taken from four patients with suspected multiple sclerosis. Patient data and clinical details are summarized in Table 1. The rapid autopsy regimen of the Netherlands Brain Bank in Amsterdam (coordinator Dr I. Huitinga) was used to acquire the samples, with

Table 1 Clinical details of multiple sclerosis and control cases

Case	Age/gender	Genotype[a]	Diagnosis	Duration, years	PM delay, h:min	Cause of death
1	69/F		PPMS/SPMS	53	7:30	Respiratory failure with heart failure
2	70/F		PPMS/SPMS	40	6:55	Urine tract infection
3	50/M		PPMS/SPMS	15	5:25	Pneumonia
4	66/F		SPMS	11	6:00	Pneumonia
5	75/F		PPMS/SPMS	24	5:00	Heart failure
6	49/M		SPMS	25	8:00	Pneumonia
7	66/M		SPMS	26	7:30	Ileus
8	64/F	Low	SPMS	31	10:10	Urinary tract infection
9	61/M	High	SPMS	18	9:15	Euthanasia
10	77/F		PPMS	24	10:00	Euthanasia
11	67/F	Mixed	SPMS	25	9:15	Palliative sedation
12	45/M		PPMS	10	7:45	Pulmonary embolism, cardiac arrest
13	59/F		SPMS	24	4:45	Euthanasia
14	58/F		SPMS	36	10:40	Euthanasia
15	44/M		PPMS	21	10:15	End stage of MS
16	51/M		SPMS	19	11:00	Unknown
17	57/F	Low	RRMS	26	8:40	Urosepsis
18	57/F	High	PPMS	29	11:00	Euthanasia
19	73/M	Mixed	RRMS	26	8:00	Urosepsis by advanced MS
20	76/F	High	SPMS	25	7:55	Euthanasia
21	56/M	Mixed	PPMS	14	9:50	Cachexia
22	74/M	Mixed	PPMS	15	10:15	Cardio-respiratory insufficiency
23	60/F	Mixed	SPMS	7	10:40	Euthanasia
24	54/M	Low	PPMS	12	8:15	Euthanasia
25	75/M	Mixed	PPMS	46	10:10	Pneumonia
26	50/F	Mixed	SPMS	17	7:35	Euthanasia
27	53/M		SPMS	24	10:00	Euthanasia
28	66/F		PPMS	13	9:35	Euthanasia
29	56/M	Mixed	SPMS	14	10:10	Suicide
30	66/F		SPMS	16	10:45	Pulmonary hypertension
31	81/F		SPMS	31	4:35	Pneumonia
32	63/M		SPMS	25	8:15	Pneumonia, cachexia, dehydration
33	75/F	High	SPMS	Unknown	9:45	Fall, subdural haematoma
34	61/F	High	Unknown	Unknown	10:00	Euthanasia
35	50/M	Low	SPMS	21	10:50	Unknown
36	49/F		Unknown	Unknown	8:30	Unknown
37	50/F		SPMS	18	9:05	Euthanasia
38	57/M		PPMS	24	10:15	Sepsis
39	35/F		SPMS	10	10:20	Euthanasia
40	54/F		Unknown	27	9:25	Respiratory failure
41	67/M		SPMS	38	11:00	Sudden death
42	54/M		SPMS	29	6:40	Euthanasia
Biopsy						
1	51/M	Demyelinating disease, suspected MS				
2	Unknown/unknown	Demyelinating disease, suspected MS				
3	27/M	Demyelinating disease, suspected MS				
4	31/F	Demyelinating disease, suspected MS				
Controls						
1	61/F		Control	N/A	6:50	Euthanasia
2	73/F		Control	N/A	4:00	Lung fibrosis and renal insufficiency
3	67/M		Control	N/A	4:30	Cardiac shock, organ failure
4	81/M		Control	N/A	5:30	Prostate carcinoma
5	67/M		Control	N/A	18:35	Myocardial infarction
6	84/F		Control	N/A	4:45	Respiratory failure
7	91/F		Control	N/A	7:45	Decompensatio cordis
8	56/M	Mixed	Control	N/A	14:00	Heart failure
9	92/F		Control	N/A	7:00	Acute death
10	62/M	Mixed	Control	N/A	7:20	Unknown
11	49/M	Mixed	Control	N/A	6:15	Euthanasia, Hodgkin's lymphoma
12	51/M		Control	N/A	7:30	Euthanasia

[a]Cases selected for autoradiography.

F = female; M = male; MS = multiple sclerosis; N/A = not applicable; PM = post-mortem; PP = primary progressive; RR = relapsing remitting; SP = secondary progressive.

the approval of the Medical Ethical Committee of the Amsterdam UMC. All participants or next of kin had given informed consent for autopsy and use of their tissues for research purposes. Tissue samples from multiple sclerosis cases were selected from regions of interest after *ex vivo* MRI (De Groot *et al.*, 2001; Bo *et al.*, 2004). Brain samples were cut in half and fixed in 10% formalin and embedded in paraffin or snap-frozen and stored in liquid nitrogen. The cases and lesions were selected from a large cohort of multiple sclerosis cases based on the size and lesion type for quantitative analysis. Lesion stages were based on immunohistochemical detection for myelin proteolipid protein (PLP) to detect areas of myelin loss and expression of human leukocyte antigen DR (HLA-DR) (van der Valk and De Groot, 2000; Kipp *et al.*, 2012). Briefly, active lesions were characterized by a focal area of myelin loss filled with myelin-laden 'foamy' macrophages; chronic active lesions were identified by a rim of activated microglia/macrophages surrounding a hypocellular centre, and inactive white matter lesions as a demyelinated area with few or no HLA-DR+ cells. The normal-appearing white (NAWM) and grey matter (NAGM) in the same tissue blocks from multiple sclerosis cases and control white and grey matter from age-matched controls were analysed as reference samples for the expression of cell markers.

Immunohistochemistry

Paraffin sections were de-paraffinized using xylene, rehydrated through descending alcohol solutions and washed in phosphate-buffered saline (PBS). Frozen sections were air-dried and fixed in 2% paraformaldehyde for 10 min at room temperature and washed in PBS. Endogenous peroxidase activity was blocked using 0.3% (w/v) H_2O_2. Following washing, paraffin sections underwent antigen retrieval in citrate or Tris/EDTA buffer in a water bath at 95°C for 30 min. After cooling, sections were washed and incubated in primary antibodies overnight in antibody diluent (Immunologic). After washing, sections were incubated in the appropriate secondary antibodies. Horseradish peroxidase labelled secondary antibodies were developed using 3,3′-diaminobenzidine (DAB, 1:50, DAKO) for 10 min after which sections were washed in Tris-buffered saline (TBS). Liquid permanent red (1:100, DAKO) was used to visualize alkaline phosphatase-labelled antibodies. Sections were washed with TBS, counterstained with haematoxylin, washed and mounted in Aquatex® (Merck). For immunofluorescence, sections were incubated with Alexa Fluor®-labelled secondary antibodies in antibody diluent for 90 min and nuclei were stained with 4′,6-diamidino-2-phenylindole (DAPI). Appropriate negative controls were used by omitting the primary antibodies.

Image and statistical analyses

Images of each lesion type and randomly sampled areas of NAWM and NAGM, and white and grey matter from controls were collected with a Leica DC500 microscope (Leica Microsystems, Heidelberg, Germany) at x200 magnification. Fluorescent images were taken with a Leica TCS SP8 STED 3X confocal microscope. Pictures were analysed using ImageJ software and nuclei and positive cells were manually counted with the cell counter plugin (de Vos, University of Sheffield, UK). All nuclei except those within blood vessels were counted to determine the number of cells per field. Expression levels were analysed using TSPO+ pixels with a threshold of signal intensity that represented all DAB+ pixels per field. Inter-observer reporting was highly consistent, with a correlation coefficient of 0.98. Data were analysed using GraphPad Prism 7.02. All data were tested for normality distribution with the Shapiro-Wilk normality test. Differences between lesion types were analysed using ANOVA or Kruskal-Wallis analyses. When positive, Dunnett's *post hoc* analysis was performed to test the different groups to their respective NAWM or NAGM and control, corrected for multiple comparisons. Accordingly, white and grey matter from control cases were compared to NAWM and NAGM of multiple sclerosis tissue, respectively. Data was considered significant when $P < 0.05$.

Genotyping

DNA extraction and genotyping were performed on snap frozen brain samples (LGC Group Ltd.). In brief, following DNA extraction, the single nucleotide polymorphism-specific KASP™ Assay mix and the universal KASP™ Master mix were added to the DNA samples and placed in a thermal cycler for a minimum of 35 cycles, producing an allele-specific fluorescent signal in accordance with primers specific to rs6971 and rs6972. Each allele-specific primer produces a unique tail sequence that is associated with a fluorescent resonant energy transfer cassette, labelled with a FAM™ dye, or HEX™ dye. Plates were read on a BMG PHERAStar plate reader (BMG Labtech). In-house Kraken software was used to automatically identify genotypes, which were verified by staff at the LGC facility.

Autoradiography

Brain sections were prepared from frozen tissue blocks corresponding to the paraffin-embedded tissue blocks described above, allowing direct comparison of the same lesion for pathology and autoradiography. Sections were cut at 10 µm and thaw-mounted on standard glass microscope slides (VWR International Ltd.). Slides were dried for 30–60 min at room temperature and stored at −80°C. At the time of use, tissue had been stored for a maximum of 36 days. Prior to autoradiography, sections were thawed at room temperature for 15 min, washed for 20 min in assay buffer (50 mM Tris-HCl, pH 7.4 and incubated for 1 h in assay buffer containing the radioligand ^{3}H-PK11195 [1-(2-chlorophenyl)-*N*-methyl-*N*-(1-methylpropyl)-3-isoquinolinecarboxamide (Perkin Elmer, specific activity 82.7 Ci/mmol)] and ^{3}H-PBR28 {*N*-[2-(methyloxy)phenyl]methyl-*N*-[4-(pheyloxy)-3-pyridinyl] acetamide (Tritec, UK, specific activity 81 Ci/mmol)}. The concentrations were 1 nmol/l for ^{3}H-PK11195 and 0.5 nmol/l for ^{3}H-PBR28 as measured by liquid scintillation counting (Beckman LS 6500).

Adjacent sections were incubated with the radioligand and 10 µmol/l PK11195 (Tocris) to determine non-specific binding. Following incubation, sections were washed twice for 2 min each in washing buffer (50 mM Tris-HCl, pH 7.4, 4°C) on ice followed by 30 s in ice-cold ultra-pure water. All slides were air dried for 15–20 min and dehydrated for a minimum of 24 h in a sealed container in the presence of phosphorous pentoxide. Slides were then exposed to BAS-TR2040 imaging plates (Fuji Film) alongside ^{3}H-standards (American Radiolabelled Chemicals) for 19 days. Imaging plates were scanned using a Typhoon FLA 7000 (GE) and analysed using Quantity One (Bio-Rad).

Autoradiography and genotyping analysis

Regions of interest were drawn around lesions, NAWM and NAGM on total binding images using immunohistochemical staining of adjacent sections as a reference. Corresponding regions of interest were drawn on the non-specific binding images for white and grey matter separately to determine the individual non-specific binding. A global background reading was obtained from a free area on the plate and subtracted from all other measurements. Radioligand signal from each area of non-specific binding was also subtracted from the corresponding ligand-bound section to eliminate non-specific signal. Radioactive concentrations were calculated from optical densities using a linear regression derived from the radioactive standards. Final values are expressed as fmol/mg tissue equivalent. The polymorphism rs6971 causes a single amino acid substitution at position 147 of TSPO, which has a substantial impact on the affinity with which PBR28 binds TSPO. The binding affinity of PBR28 for TSPO is reduced by a factor of ~50 in subjects with threonine at position 147 (termed 'low affinity binders') relative to subjects with alanine at position 147 (termed 'high affinity binders'). Heterozygotes (termed 'mixed affinity binders') express both copies of TSPO (Ala147 and Thr147) and hence present both the high and low affinity binding sites in roughly equal proportion. Therefore, for a given expression level of the TSPO protein detected by immunohistochemistry, the ^{3}H-PBR28 radioligand binding signal will be genotype dependent, showing rank order high affinity binders > mixed affinity binders > low affinity binders. Including all three genotypes in a correlation of the ^{3}H-PBR28 signal with immunohistochemistry would therefore artificially weaken the correlation, and hence for this analysis, only high affinity binders were used. This phenomenon is not relevant for ^{3}H-PK11195 as the affinity of this radioligand for TSPO is insensitive to the Thr147/Ala147 substitution.

Mean ligand binding for each region of interest was calculated. For sections containing multiple regions of interest for the same tissue type, the mean was calculated. Data were analysed using GraphPad Prism 7.02 (GraphPad Software, San Diego, CA). Data were tested for normality distribution with the Shapiro-Wilk normality test. Differences between lesions were analysed using a Kruskal-Wallis analysis with Dunnett's *post hoc* analysis and considered significant when $P < 0.05$.

Data availability

The data that support the findings of this study are available from the corresponding author on reasonable request.

Results

Heterogeneity of TSPO + cells in multiple sclerosis lesions

Expression and localization of TSPO + cells were investigated in NAWM and in active, chronic active and inactive white matter lesions from brains and spinal cord of people with multiple sclerosis and in control tissue from people who died of non-neurological diseases (Fig. 1A–F). TSPO immunostaining had a punctate appearance across the cytoplasm of cells in both the controls and in cells from multiple sclerosis tissue, as is expected with a mitochondrial protein. The density of TSPO + cells/mm^2 was 5-fold greater in active white matter lesions ($P < 0.0001$) and 4-fold greater in rims of chronic active brain lesions ($P = 0.0001$) compared to control white matter. Compared to NAWM, the density of TSPO + cells was a mean of 2-fold higher for active lesions ($P = 0.004$) and chronic active lesions ($P = 0.0170$, Fig. 1G).

We next investigated the characteristics of the TSPO + cells. HLA-DR + cells expressing TSPO were 11- to 14-fold more abundant in active lesions and chronic active lesion rims compared to the control white matter (active: $P = 0.0220$, chronic active rim: $P = 0.0022$; Fig. 1H) and 16- to 21-fold greater than NAWM (active: $P = 0.0196$, chronic active rim: $P = 0.0019$, Fig. 1H). TSPO + HLA-DR− cells with an astrocytic morphology expressing GFAP were found in all lesion subtypes (Fig. 1I–N). Between 15- to 20-fold more TSPO + GFAP + cells were observed in all lesion subtypes relative to control white matter ($P < 0.0001$, Fig. 1O). The relative number of TSPO + GFAP + cells in lesions was 5- to 7-fold greater than in the NAWM ($P < 0.0001$, Fig. 1O).

HLA-DR + microglia/macrophages expressing TSPO accounted for a mean of 40% of total TSPO + cells in active lesions and in the rims of chronic active lesion (Fig. 1P) and GFAP + astrocytes constituted about 25% of TSPO + cells in active lesions and in the rims of chronic active lesions. However, in the centre of chronic active and in inactive lesions TSPO + GFAP + astrocytes represented as many as 65% of the TSPO + cells although it must be emphasized that the centre of these lesions are hypocellular relative to the chronic lesion rims or the NAWM. In active lesion areas, a few cells were found co-expressing TSPO and OLIG2, an oligodendrocyte marker (Fig. 1P, inset). TSPO + astrocytes did not only co-localize with GFAP but also with vimentin, glut-1 and S100β (Fig. 1Q–T). Most of the remaining fraction of TSPO + cells that did not express HLA-DR or GFAP had microglial or macrophage morphology, but were not further characterized. To examine if the same is true of lesions in early multiple sclerosis, we used biopsy material from rapidly expanding active white matter lesions from four cases of multiple sclerosis. All samples also showed strong expression of TSPO in HLA-DR + macrophages and microglia (Fig. 1U), as well as in scattered GFAP + astrocytes (Fig. 1V).

Together, microglia and, to a lesser extent, astrocytes in multiple sclerosis lesions appeared to account for most of the TSPO + cells in lesions and NAWM in the multiple sclerosis brains. TSPO + vascular endothelial cells also were identified commonly but made up <5% of the TSPO + cells. Vascular TSPO expression patterns in multiple sclerosis lesions were not different from their expression in blood vessels of the NAWM and in control tissue.

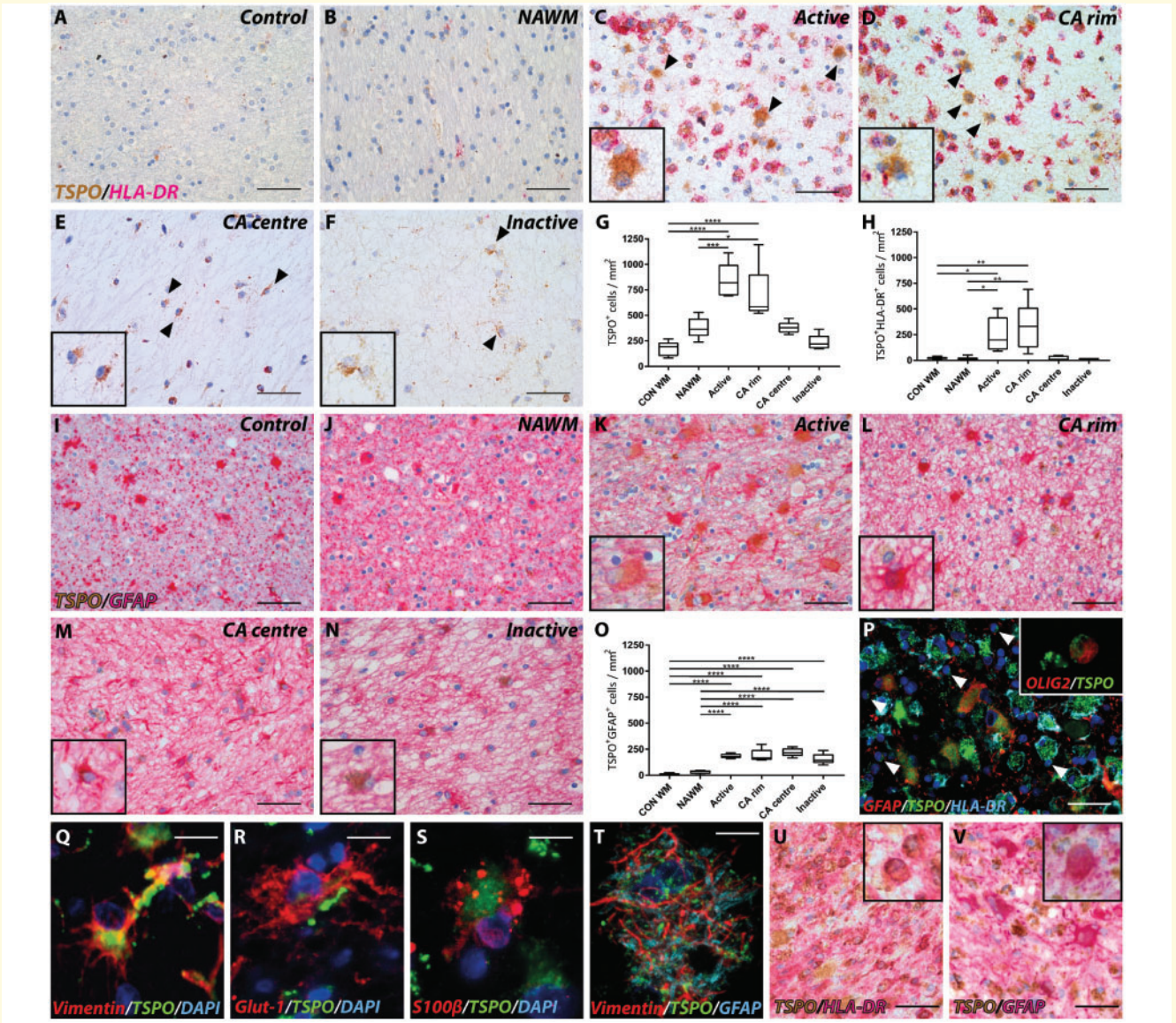

Figure 1 Astrocyte and microglial expression of TSPO in white matter lesions. Representative images of TSPO expression in control (**A** and **I**) and multiple sclerosis lesions (**B**–**F** and **I**–**N**); NAWM (**B** and **J**), active (**C** and **K**), chronic active (CA) rim (**D** and **L**) and centre (**E** and **M**), and inactive (**F** and **N**) lesions. Expression of TSPO in HLA-DR− cells (black arrowheads; insets **C**–**F**). Quantitative analysis of number of TSPO + cells showed a significant increase up to five times in active and in the rim of chronic active lesions compared to control and NAWM (**G**). An 11- to 14-fold increase in TSPO + HLA-DR + cells was found in active and the rim of chronic active lesions compared to control and NAWM (**H**). A 5-fold increase in TPSO + GFAP + cells was found throughout all lesion stages compared to control and NAWM contributing up to 25% of the TSPO + cells (**I**–**O**, insets). An overview of cellular TSPO signal of astrocytes and activated microglia macrophages (**P**) and oligodendrocytes (**P**, white arrowheads, inset). Representative images of astrocytic markers with TSPO expression in one multiple sclerosis lesion (**Q**–**T**). Biopsy material showing high TSPO expression in HLA-DR + and GFAP + cells (**U** and **V**, inset). $^{*}P < 0.05$; $^{**}P < 0.01$; $^{***}P < 0.001$; $^{****}P < 0.0001$. Scale bars in **A**–**F**, **I**–**N**, **P**, **U** and **V** = 50 μm; **Q**–**T** = 12.5 μm. Insets are digitally zoomed to ×800.

TSPO expression in microglial phenotypes

To investigate whether TSPO expression in microglial cells defined a functionally specific phenotype, we tested for co-expression with more specific markers for microglia and their polarization. TMEM119 is reported to differentiate activated microglia from myeloid-derived macrophages and has been used to identify CNS-resident microglia. P2RY12 is a marker that identifies homeostatic microglia in normal white matter. Markers for pro-inflammatory (CD40) and anti-inflammatory (mannose receptor, CD206) activated microglia and macrophages also were used (Vogel *et al.*, 2013; Giles *et al.*, 2018). Microglia/

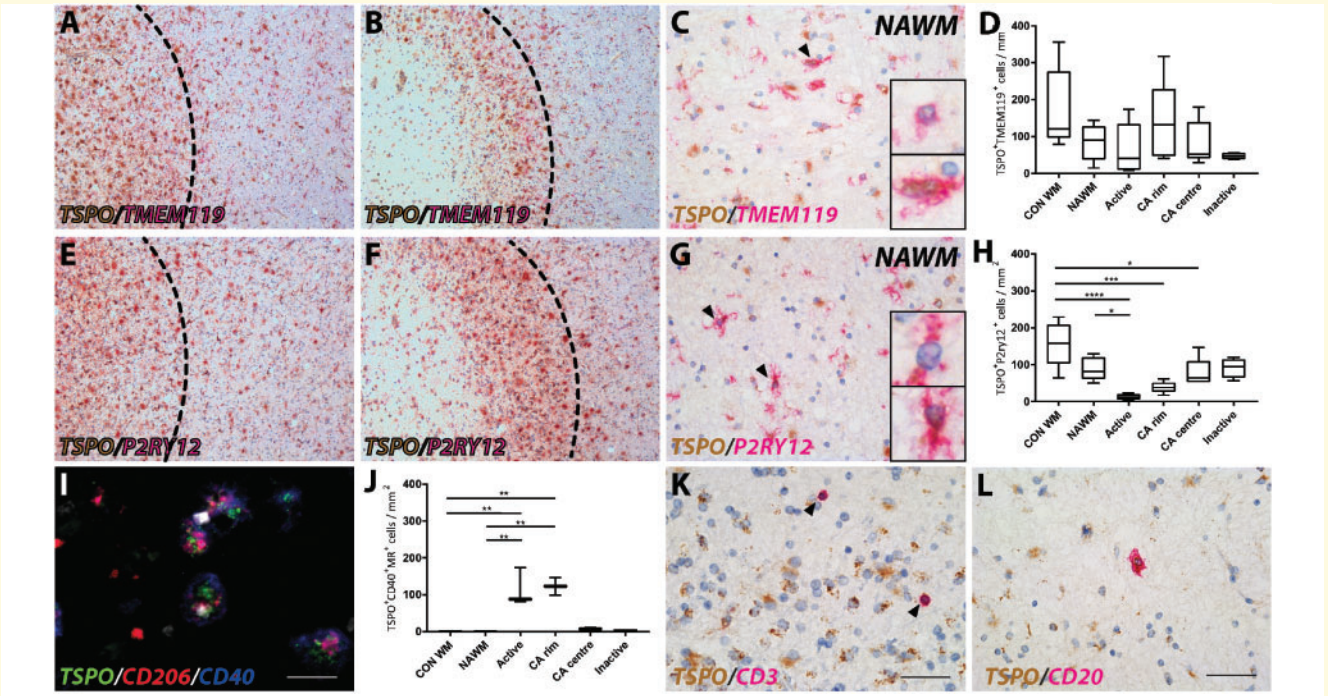

Figure 2 TSPO expression in microglial phenotypes and lymphocytes. Resident microglia expressing TSPO in an active and chronic active lesion and the periplaque white matter (**A** and **B**) as well as in NAWM (**C**). Resident microglia did not show any significant difference in TSPO expression compared to control or NAWM (**D**). Overview of expression of the homeostatic marker P2RY12 with TSPO in an active and chronic active lesion and the periplaque white matter (**E** and **F**), as well as in NAWM (**G**). A loss in homeostatic microglia expressing TSPO was found in active and chronic active lesions stages (**H**). Both TSPO + and TSPO− microglia were found expressing TMEM119 or P2RY12 in multiple sclerosis lesions (black arrowheads; insets; **C** and **G**). In contrast, active and chronic active lesions showed an increase in CD206 + CD40 + cells expressing TSPO (**I** and **J**). T cells (CD3) showed low expression of TSPO in multiple sclerosis lesions (**K**) in contrast to B cells (CD20) which showed strong localization with TSPO (**L**). $^{*}P < 0.05$; $^{**}P < 0.01$; $^{***}P < 0.001$; $^{****}P < 0.0001$. Scale bars in **A**, **B**, **E** and **F** = 200 μm; **C**, **G**, **K** and **L** = 50 μm, **I** = 25 μm. Insets are digitally zoomed to ×800. CA = chronic active.

macrophages that express both CD40 and CD206 are described as having an intermediate phenotype. No significant differences were found in proportions of TMEM119 + microglia expressing TSPO across the lesion subtypes (Fig. 2A–D). As reported previously (Zrzavy *et al.*, 2017), P2RY12 + cells expressing TSPO were substantially reduced in active lesions (Fig. 2E–H). Numbers of macrophages and microglia showing an intermediate phenotype, and expressing TSPO were very low in control cases and were not detected in the NAWM in multiple sclerosis (Fig. 2I and J). The density of microglia/macrophages with the intermediate phenotype represented 18% of the total TSPO + cell population, in active lesions and in the rims of chronic active lesions (Fig. 2J). By contrast, few TSPO + microglia/macrophages with the intermediate phenotype were present in the centres of chronic active lesions or in inactive lesions, (Fig. 2J). Cells that were solely expressing the pro-inflammatory marker CD40 or the anti-inflammatory mannose receptor CD206 always expressed TSPO, but were present in very low numbers in multiple sclerosis lesions (<1% of total TSPO + cells, data not shown). Thus, TSPO expression was not specifically associated with either solely pro- or anti-inflammatory microglia/macrophage phenotype based on these markers.

TSPO expression in lymphocytes

Expression of TSPO in adaptive immune cells was investigated by double staining CD20 + B cells and CD3 + T cells in white matter lesions in multiple sclerosis (Fig. 2K and L). The density of TSPO expression in CD3 + T cells was very low in all lesion types (Fig. 2K) compared to expression by microglia. CD20 + B cells showed relatively stronger expression of TSPO in active (Fig. 2L), chronic active and inactive lesion types. However, in the cases studied in this study T- and B-cell numbers were low in multiple sclerosis lesions and in the NAWM, and did not contribute significantly to the total number of TSPO + cells (<1% of total TSPO + cells).

TSPO expression in multiple sclerosis lesions in the cortical grey matter and spinal cord

Expression and localization of TSPO in the grey matter of multiple sclerosis brain was investigated in leukocortical, intracortical, subpial and transcortical lesions (Fig. 3A–I) (Bo, 2009). No significant differences were found in the number of cells that express TSPO in grey matter lesions

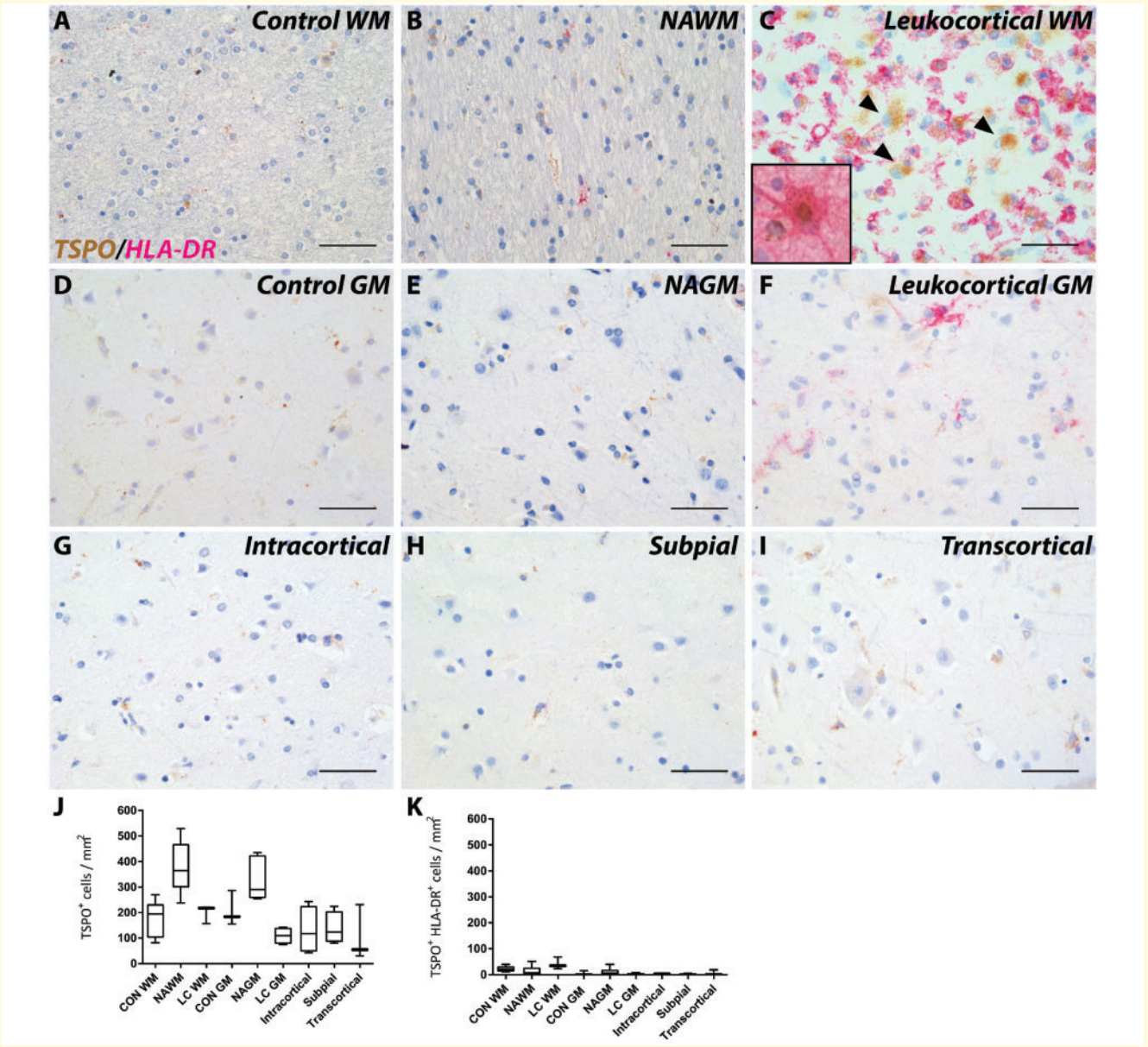

Figure 3 TSPO expression in grey matter lesions. Representative images of TSPO expression in control (**A** and **D**) and multiple sclerosis (**B**, **C** and **E**–**I**) in grey matter lesions; NAWM (**B**), and NAGM (**E**); leukocortical white matter (**C**), and grey matter (**F**); intracortical (**G**), subpial (**H**), and transcortical (**I**) lesions. Similar to white matter lesions leukocortical white matter lesions showed large TSPO + HLA-DR− cells (black arrowheads; **C**) which were GFAP + astrocytes (**C**, inset). No differences were found in TSPO + cells in grey matter lesions (**J**). No significant increase in TSPO + HLA-DR + cells were found in grey matter lesions compared to control (**K**). Data are expressed as mean ± SEM. Scale bars in **A**–**I** = 50 μm. Insets are digitally zoomed to × 800. CON = control; GM = grey matter; LC = leukocortical; WM = white matter.

compared to NAGM or to control grey matter (Fig. 3J). HLA-DR + cells expressing TSPO were not significantly more abundant in the white and grey matter of leukocortical lesions than in the normal appearing white and grey matter or to control tissue (Fig. 3K) and the density of TSPO + HLA-DR + microglia was low compared to white matter lesions. We observed scattered GFAP + astrocytes expressing TSPO only in the white matter of leukocortical lesions, similar to those found in purely white matter lesions (Fig. 3C, inset).

The density of TSPO + cells in the NAWM of the spinal cord was no greater than in control spinal cord white matter and neither was the TSPO + cell density greater in white matter lesions in the spinal cord compared to NAWM or control white matter (Fig. 4A–F). However, the density of TSPO + HLA-DR + cells in active white matter lesions was approximately doubled relative to control white matter (P = 0.0324; Fig. 4G). Active and chronic active lesions in the spinal cord also showed GFAP + astrocytes expressing TSPO similar to the brain (Fig. 4C and D, inset).

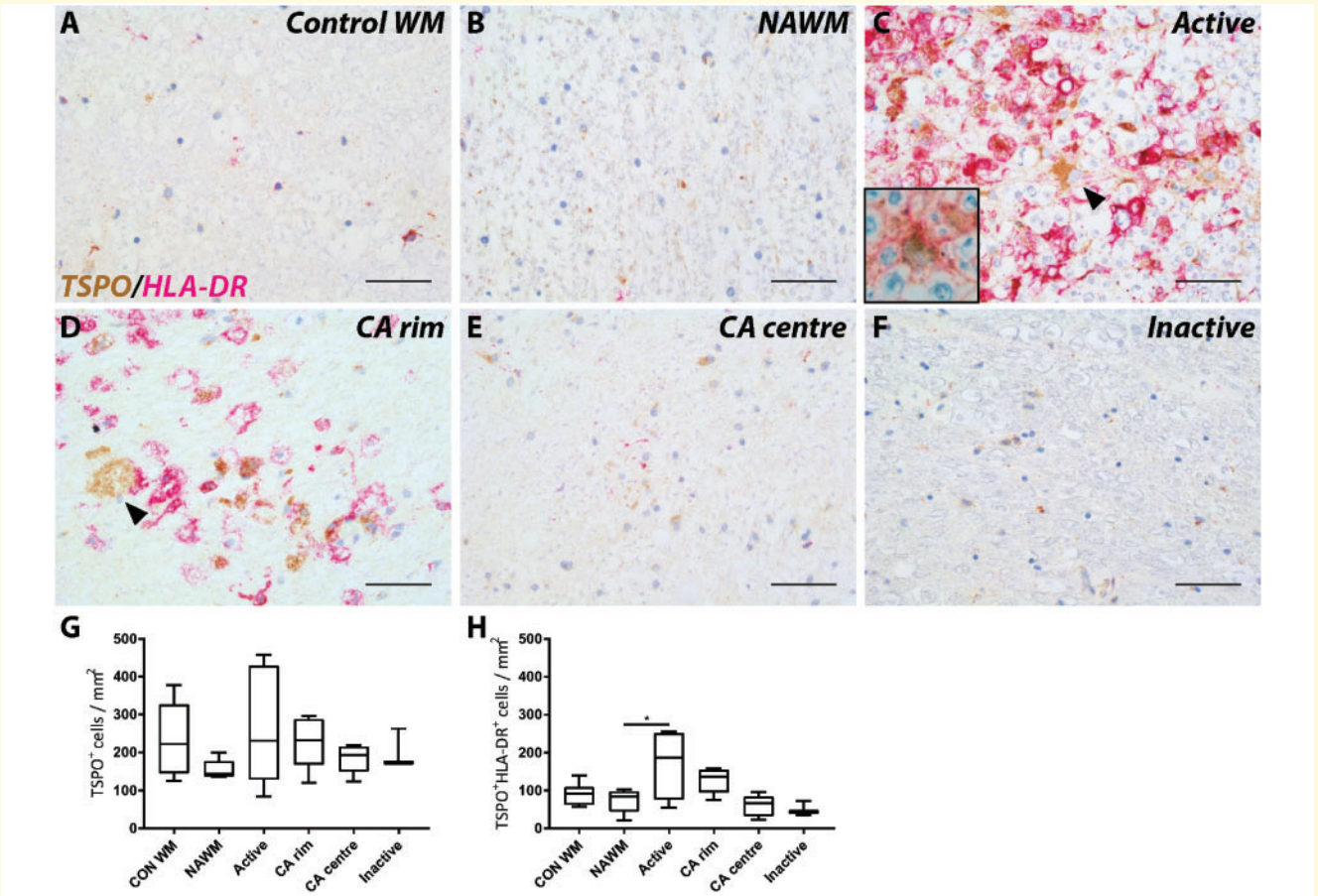

Figure 4 TSPO expression in white matter lesions in spinal cord. Representative images of TSPO expression in control (**A**) and multiple sclerosis lesions (**B**–**F**); NAWM (**B**), active (**C**), chronic active (CA) rim (**D**) and centre (**E**), and inactive (**F**) lesions. Expression of TSPO was found in HLA-DR$^-$ cells (black arrowheads; **C** and **D**). GFAP+ astrocytes expressing TSPO were also found in the spinal cord (**C**, inset). Quantitative analysis of the number of TSPO+ cells did not show significant differences between lesion types compared to control or NAWM (**G** and **H**). Increased expression of TSPO in HLA-DR+ cells was found in active lesions compared to NAWM (**I**). $^*P < 0.05$. Scale bars in **A**–**F** = 50 μm. Insets are digitally zoomed to ×800. A = active; CON = control.

TSPO pixels and radioligand binding are increased in active lesions

To investigate the relationship between TSPO expression and radioligand binding of ^{3}H-PBR28 or ^{3}H-PK11195, results from a pixel-based analysis of immunochemically-defined TSPO were integrated with TSPO radioligand autoradiography of white and grey matter lesions from sections in the same tissue blocks from multiple sclerosis and control brains (Fig. 5). In white matter lesions, the number of TSPO+ pixels were increased by 5-fold compared to control white matter (active: $P < 0.0001$; chronic active rim: $P = 0.0003$) and by 9-fold compared to NAWM (active: $P < 0.0001$; chronic active rim: $P < 0.0001$; Fig. 6A). Endothelial TSPO expression contributed minimally (up to 8% in inactive lesions) to the amount of TSPO+ pixels in the white matter (Supplementary Fig. 1A).

TSPO+ pixels were found to be increased markedly in the white matter component of leukocortical lesions relative to NAWM ($P < 0.0001$, Fig. 6D) and to control white matter ($P < 0.0001$). A smaller increase in TSPO+ pixels was found in the grey matter ($P = 0.0096$) of leukocortical lesions relative to NAGM. However, no significant increase in TSPO+ pixels was found in other subtypes of grey matter lesions. Endothelial TSPO expression was decreased in grey matter lesions compared to the NAGM ($P < 0.005$) and control grey matter ($P < 0.05$, Supplementary Fig. 1B). Furthermore, endothelial TSPO expression was up to a 4-fold higher in the NAGM and control grey matter compared to NAWM ($P < 0.0001$) and control white matter ($P = 0.0033$) in the brains of patients with multiple sclerosis (Supplementary Fig. 1B).

Specific tracer binding was calculated from ^{3}H-PBR28 and ^{3}H-PK11195 autoradiography in lesional and non-lesional areas of white and grey matter in the multiple sclerosis brains and in control tissue (Fig. 5). No specific binding was found in four brains with low affinity binding genotypes for ^{3}H-PBR28, identified by the rs6971

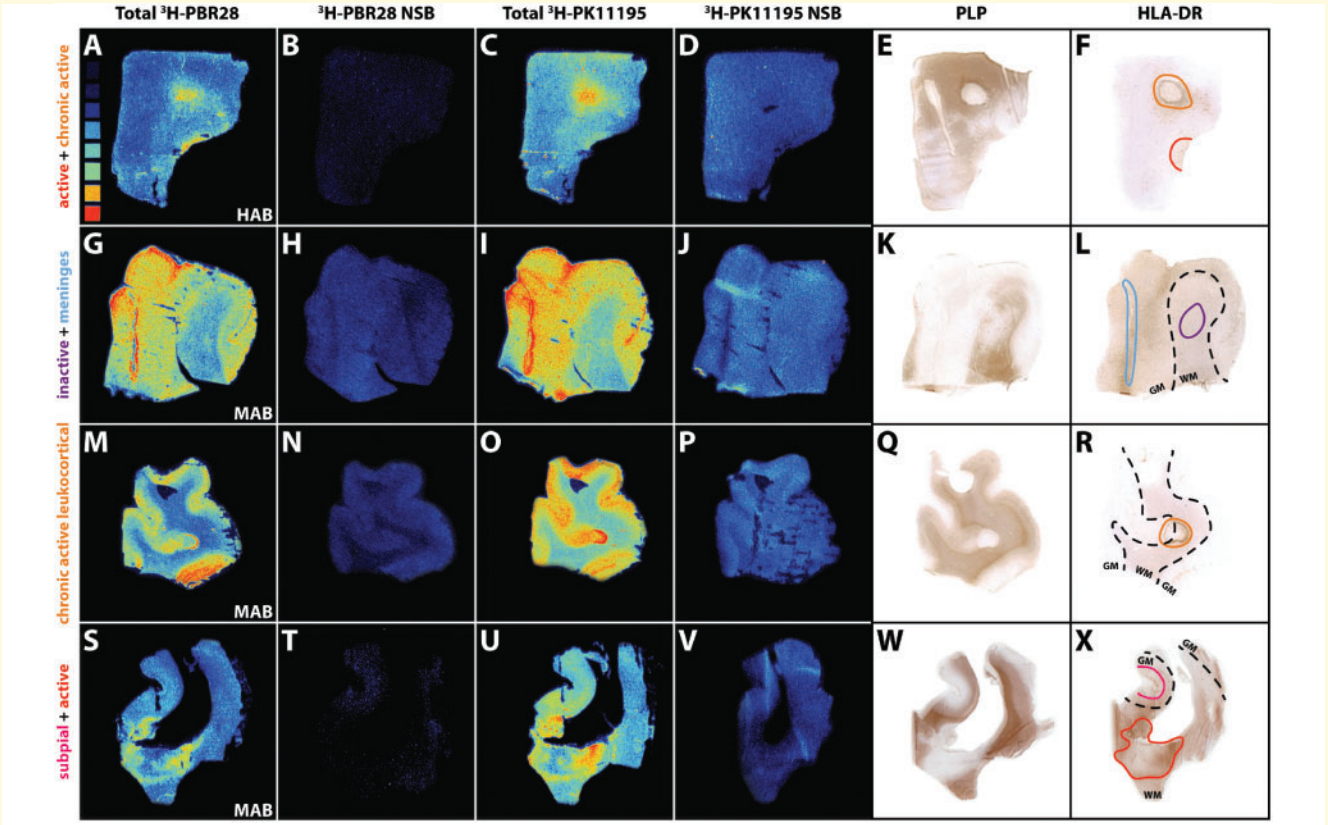

Figure 5 Overview of ^{3}H-PBR28 and ^{3}H-PK11195 autoradiography of multiple sclerosis lesions. Heat map in **A** ranges from low to high radioactivity (0.42 tissue equivalent nCi/mg to 16.23 tissue equivalent nCi/mg). Total binding of ^{3}H-PBR28 (**A**, **G**, **M** and **S**), non-specific binding of ^{3}H-PBR28 (**B**, **H**, **N** and **T**), total binding of ^{3}H-PK11195 (**C**, **I**, **O** and **U**), non-specific binding of ^{3}H-PK11195 (**D**, **J**, **P** and **V**), PLP (**E**, **K**, **Q** and **W**) and HLA-DR (**F**, **L**, **R** and **X**) images. LN3 staining denotes areas for active (red), chronic active (orange), inactive (purple) and subpial (pink) lesions, meninges (blue) and the grey and white matter border (dashed lines).

polymorphism. In all other cases, control white matter, NAWM and inactive lesions all showed relatively low binding of both ligands compared to active and chronic active lesions (Fig. 6B and C). ^{3}H-PBR28 binding was seven times greater in active lesions compared to control white matter (P = 0.0228) and three times greater than NAWM (P = 0.0064). Similarly, greater binding was found in the centres of chronic active lesions compared to NAWM (P = 0.0046) or control white matter (P = 0.0084, Fig. 6B). ^{3}H-PK11195 binding was approximately doubled in the active (P = 0.0006) and tripled in the chronic active centre (P = 0.0392) compared to NAWM (Fig. 6C). In grey matter lesions (Fig. 6E and F), binding was not greater for either ^{3}H-PBR28 or ^{3}H-PK11195 than in NAGM. An increased signal was found in the white matter of leukocortical lesions compared to control (P = 0.0414) for ^{3}H-PBR28 or compared to NAWM (P = 0.0019) for ^{3}H-PK11195. Specific binding in NAGM was more than tripled relative to NAWM for ^{3}H-PBR28 (P = 0.0009).

A strong positive correlation between the pixel-based analysis of TSPO expression and specific binding of the ligand ^{3}H-PBR28 was found (R^2 = 0.5017, P = 0.0327), while only a trend was found for ^{3}H-PK11195 (R^2 = 0.4417, P = 0.0509, Fig. 6G). Strong correlations were also found between the relative number of TSPO+ cells and specific binding for ^{3}H-PBR28 (R^2 = 0.4698, P = 0.0139) and ^{3}H-PK11195 (R^2 = 0.3229, P = 0.0271, Fig. 6H).

Discussion

TSPO is a marker of inflammation commonly attributed to microglial activation in neuroinflammatory and neurodegenerative diseases (Guilarte, 2019). Surprisingly, there has been very little data on which to base precise interpretations to date (Matthews and Datta, 2015). Knowledge of the cellular and phenotypic correlates of the TSPO PET signal is important to better understand the clinical meaningfulness of the heterogeneity of TSPO PET radioligand uptake in T_2-hyperintense lesions in multiple sclerosis before and after initiation of disease modifying therapies (Datta *et al.*, 2017*a*).

Here we have examined the expression and localization of TSPO in a large cohort of post-mortem multiple sclerosis in white and grey matter lesions of the brain and spinal cord. Similar to previous studies, TSPO expression was

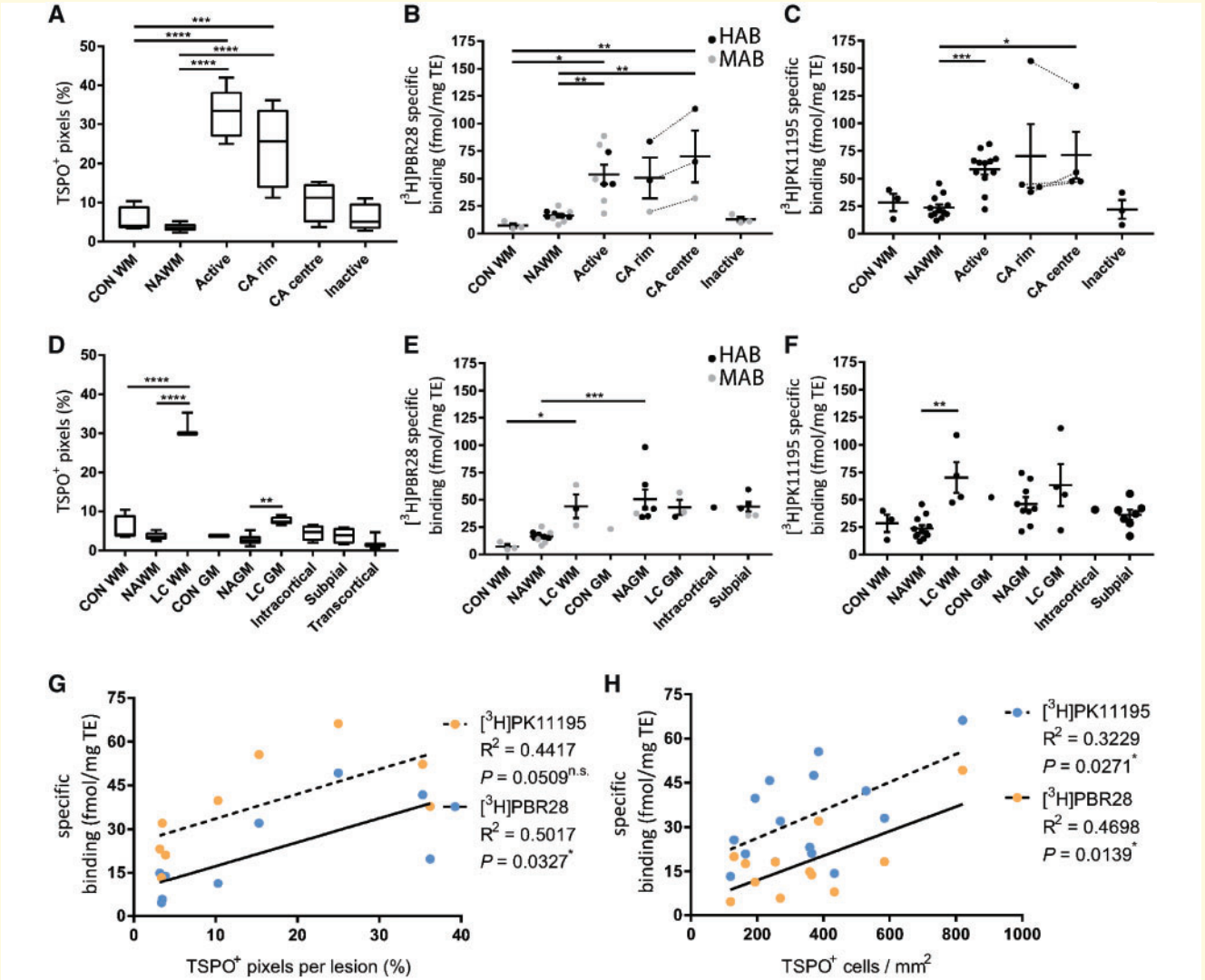

Figure 6 ^{3}H-PBR28 and ^{3}H-PK11195 autoradiography of multiple sclerosis lesions. An increase in TSPO + pixels was found in active and chronic active lesions compared to control and NAWM (**A**). ^{3}H-PBR28 and ^{3}H-PK11195 binding was increased in active white matter lesions and the centre of chronic active lesions (**B** and **C**). For grey matter lesions an increase was found in TSPO + pixels in leukocortical lesion white matter and grey matter compared to their respective normal appearing tissue (**D**). Similar to white matter lesions ^{3}H-PBR28 and ^{3}H-PK11195 binding was increased in leukocortical lesion white matter areas (**E** and **F**). An increase in specific binding in NAGM relative to NAWM was found for ^{3}H-PBR28. Mixed affinity binders (MAB) are depicted in grey while high affinity binders are depicted in black (HAB). Correlations were found for specific binding of ^{3}H-PBR28 and ^{3}H-PK11195 for both TSPO + pixels per lesion and TSPO + cells/mm^{2} (**G** and **H**). CA = chronic active; CON GM = control grey matter; CON WM = control white matter; LC = leukocortical lesion; TE = tissue equivalent.

found in microglia in active and chronic active lesions (Cosenza-Nashat *et al.*, 2009; Martin *et al.*, 2010; Lavisse *et al.*, 2012*a*; Loth *et al.*, 2016; Kaunzner *et al.*, 2019). Similar to a recent study combining quantitative susceptibility mapping and immunohistochemistry (Kaunzner *et al.*, 2019), our studies revealed non-trivial expression of TSPO in astrocytes in all subtypes of lesions examined. The astrocytic TSPO accounted for ~25% of the TSPO + cells in active lesions or chronic active lesion rims and for 65% of the TSPO + cells in the centres of chronic active and inactive lesions. Autoradiography using ^{3}H-PBR28 and ^{3}H-PK11195 revealed a strong correlation between TSPO + cells and radioligand binding across all cell subtypes. This suggests that the TSPO PET signal arises from astrocytes as well as microglia, which is consistent with reports that newer generation ligands for TSPO bind to reactive astrocytes (Dickens *et al.*, 2014; Kaunzner *et al.*, 2019). Interpretation of the signal therefore needs to be context dependent. This finding is of clear importance for use of TSPO PET as an outcome measure in studies of modulation of these inflammatory processes.

While some studies have found reduced TSPO binding after anti-inflammatory treatments (Ratchford *et al.*, 2012; Sucksdorff *et al.*, 2017), it has also been suggested

that current disease-modifying therapy may have a limited impact on microglial activity (Datta *et al.*, 2017*a*; Bunai *et al.*, 2018). However, as centres of chronic active and inactive lesions show increased expression of TSPO in reactive astrocytes, observations of TSPO expression alone are more ambiguous; treatment may reduce microglial density or activation without a reduction in TSPO PET signal, if astrocytic numbers increase simultaneously. The astrocytic contribution of the TSPO signal could also complicate differentiation of multiple sclerosis from leukodystrophies that have significant astrocytic but not microglial involvement (van der Knaap and Bugiani, 2017).

While percentages of microglia in the grey matter have been reported to be significantly higher in white versus grey matter (Mittelbronn *et al.*, 2001) an increase of radioligand binding in the NAGM compared to the NAWM was observed. This may be attributed to the increased contribution of TSPO+ endothelial cells due to the reported increased vascularity of grey verses white matter (Hase *et al.*, 2019). That TSPO protein expression does not correlate with the PBR28 findings in the grey matter likely reflects the fundamentally different measurements of antibody binding (pixel counts) and autoradiography (ligand binding); the antibody detects the C terminus of the TSPO and autoradiography the binding of the ligand in the active site of the TSPO. Autoradiography has greater sensitivity because each molecule of radioligand contributes to the signal, whereas for immunohistochemistry a pixel is only TSPO+ if a threshold is reached. Hence when the levels of TSPO are low, and thus the signal of DAB positivity is very low, differences between autoradiography and the pixels counts may arise.

Increased TSPO expression was also observed in leukocortical lesions in multiple sclerosis but not in other grey matter lesions (Bo *et al.*, 2003). This may well reflect the greater microglia and astrocyte activity in the white matter; pure cortical lesions in post-mortem tissues show little or no inflammation (Bo *et al.*, 2004; Brink *et al.*, 2005; van Horssen *et al.*, 2007), although early lesions have been associated with prominent microglial activation (Lucchinetti *et al.*, 2011). Leukocortical lesions, which can have a white matter inflammatory component, may show differences in behaviour with inflammatory processes diffusing into the cortical grey matter. Similar considerations may hold with active leptomeningeal inflammation (Howell *et al.*, 2011; Absinta *et al.*, 2015). The spatial resolution of PET is low relative to cortical thickness, making confident assignment of TSPO PET signal to cortex (rather than adjacent white matter or meninges) problematic. While populations of patients undoubtedly show heterogeneity of grey matter pathology, our observations here raise questions about the interpretation of widespread TSPO PET signal in the cortical region as arising from cortical lesions (Politis *et al.*, 2012), as opposed to meningeal (Howell *et al.*, 2011) or leukocortical inflammation. Highly localized relative increases in TSPO signal in the cortex (Herranz *et al.*, 2016), may represent a rarer, relatively acute cortical lesion, rather than what is more typically defined post-mortem.

Increased TSPO expression also has been commonly attributed to activated microglia/macrophages and there is often an implication that the activation is pro-inflammatory (Guilarte, 2019). Recently, we have shown *in vitro* that, although TSPO gene and protein expression and TSPO radioligand binding increases in rodent microglia and macrophages with inflammatory stimulation, relative *TSPO* gene expression in human microglia and TSPO ligand binding in human monocyte-derived macrophages are reduced with pro-inflammatory activation (Owen *et al.*, 2017). Here, we show that the increased TSPO expression in multiple sclerosis lesions primarily represents an intermediate activation state in which cells expressed both CD40 and CD206 (Vogel *et al.*, 2013; Peferoen *et al.*, 2015); microglia solely expressing the pro-inflammatory marker CD40 or the anti-inflammatory marker mannose receptor CD206 were sparsely represented. This new observation thus confirms *in vitro* data suggesting that the TSPO expression signal does not distinguish between microglial phenotypes in human tissue (Owen *et al.*, 2017). To the extent that increased TSPO PET signal can be used as a marker of microglia, it thus should be interpreted as reflecting increased microglial density rather than a change in activation state.

In principle, chronic active lesions showing a high expression of TSPO in the rims and a lower expression in the core could be distinguished from either active lesions that show high expression of TSPO throughout their volume or from inactive lesions with low cell density and low TSPO expression. Those chronic active lesions with increased rim TSPO expression might identify those that will expand slowly over time. The neuropathological active lesions with homogeneously high TSPO expression may define those most likely to decrease in volume over time (Sethi *et al.*, 2017; Elliott *et al.*, 2018). However, in practice, this discrimination could be confounded by the limited signal resolution of PET (typically 3–5 mm linearly) and consequent local signal averaging across commonly encountered lesions. This question deserves further investigations, e.g. by combining longitudinal MRI monitoring of the evolution of individual lesions with TSPO PET.

In the present study, TSPO expression in cells of the adaptive immune system was also investigated across the different lesion subtypes. A previous study has highlighted TSPO expression in several T-cell populations in blood (Harberts *et al.*, 2013), but our study did not find a strong expression of TSPO in T cells in the brain. On the other hand, we did see strong expression of TSPO in B cells in active, chronic active, and inactive lesions. However, lymphocyte numbers are low, so these contribute only a negligible amount to the total TSPO+ cells and thus will not influence the TSPO PET signal significantly.

TSPO expression in vascular endothelial cells in all blood vessels contributes to the diffuse TSPO PET signal in the healthy human brain (Veronese *et al.*, 2018). Moreover, the endothelial component of TSPO PET, which is dependent on

Table 2 Antibodies for immunohistochemistry

Antigen	Source	Antibody	Species	Dilution
TSPO (PBR)	Abcam	AB109497	Rabbit	1:750
PLP	Bio-Rad	MCA839G	Mouse	1:3000
HLA-DR (LN3)	BioLegend	327011	Mouse	1:1000
Vimentin	Homemade	N/A	Mouse	1:6000
GFAP	Millipore	AB5541	Chicken	1:1000
Olig2	Millipore	AB9610	Rabbit	1:500
CD3	Agilent	A0452	Rabbit	1:1500
CD20	Agilent	M0755	Mouse	1:100
TMEM119	Merck	HPA051870	Rabbit	1:250
P2RY12	ANASPEC	AS55042A	Rabbit	1:200
CD40	Bio-Rad	MCA1590	Mouse	1:50
Mannose receptor (CD206)	BD Biosciences	555953	Mouse	1:50
S100β	Merck	S2532	Mouse	1:200
GLUT-1	Merck	AB1783	Guinea pig	1:100

GLUT-1 = glucose transporter.

the vascular density in the brain, differs between regions, and may change with ageing and pathology (Mann *et al.*, 1986; Veronese *et al.*, 2018; Wimberley *et al.*, 2018). We therefore investigated TSPO expression in endothelial cells by pixel count. In the white matter, endothelial TSPO expression did not contribute significantly to the total amount of TSPO expression (on average 5% of total TSPO pixels). However, as expected, we found an increase in endothelial contribution to TSPO expression relative to white matter as well as relative to grey matter lesions, which is consistent with the reported greater vascularity of grey verses white matter (Hase *et al.*, 2019) and the hypocellularity of grey matter lesions (Bo, 2009).

The abundance of TSPO expression in astrocytes in the centres of chronic active lesions may suggest a more important role for TSPO in the pathophysiology of multiple sclerosis than previous data suggested (Cosenza-Nashat *et al.*, 2009). The human GFAP-driven conditional knockout of TSPO in mice resulted in significantly reduced severity of experimental autoimmune encephalomyelitis (Daugherty *et al.*, 2016). In humans, activated microglia are capable of producing neurotoxic, reactive astrocytes in multiple sclerosis lesions (Liddelow *et al.*, 2017). The apparent effects of TSPO ligands to reduce pathology in animal disease models could be mediated through effects on astrocytes (Ryu *et al.*, 2005; Veiga *et al.*, 2005). Similar to TSPO expression after cessation of lesion activity in multiple sclerosis, TSPO was found to be expressed long after recovery from experimental autoimmune encephalomyelitis and in cuprizone-mediated demyelination (Agnello *et al.*, 2000; Chen and Guilarte, 2006), implicating a role of TSPO in regenerative processes such as remyelinating lesions, possibly through production of neurotrophic factors such as pregnenolone and progesterone (Le Goascogne *et al.*, 2000). These activities may be mediated by activated astrocytes.

There are limitations to our study suggesting future work. HLA-DR, Iba1 and CD68 are often used as markers for microglia interchangeably. Although these markers may be co-expressed, some Iba1+ and CD68+ cells do not express HLA-DR (Hendrickx *et al.*, 2017). This likely accounts for the TSPO+ cells with microglial morphology that did not express HLA-DR. These appear to constitute a fraction of up to 35% of the active lesions and the chronic active lesion rims, but confirmation of this is warranted. A more general problem is that characterization of the complexity of microglial/macrophage activation phenotypes well ideally demands use of more than one or two markers. Future work using cytokine expression assays and cell receptor markers simultaneously (e.g. using imaging mass cytometry) would add to their characterization.

In summary, our studies confirm that TSPO PET imaging provides a general marker of glial activation in multiple sclerosis, but emphasize that precise interpretations depend on the specific pathological context. With a single MRI scan, active, chronic active and inactive lesions cannot be distinguished well, leaving uncertainties regarding the interpretation of a paired TSPO PET scan. With other pathologies e.g. in Alzheimer's disease (Okello *et al.*, 2009), the interpretation of increased TSPO PET signal also may reflect differences in relative abundance of microglia and astrocytes. Based on this and our previous work, we raise the possibility that a successful therapeutic intervention, which modulates the microglia from pro-inflammatory to neuroprotective or homeostatic phenotypes, might potentially have no effect on the TSPO PET signal, although interventions that reduce the density of activated glial cells may. Understanding the cellular neuropathology of TSPO expression quantitatively is a fundamental step in the evaluation of TSPO as a potential therapeutic target.

Funding

The authors thank the UK MS society for financial support (grant number: C008-16.1). P.M.M. acknowledges generous support from Edmond J Safra Foundation and Lily

Safra, the NIHR Investigator programme and the UK Dementia Research Institute. P.M.M. and D.R.O. thank the Imperial College Healthcare Trust-NIHR Biomedical Research Centre for infrastructure support and the Medical Research Council for support of TSPO studies (MR/N008219/1 and MR/N016343/1).

Competing interests

P.M.M. acts as a scientific advisor to Ipsen Pharmaceuticals and has served on advisory boards or received speakers' honoraria from Biogen, Roche, Celgene and Novartis. He has received research or educational support from Biogen, Novartis and GlaxoSmithKline.

Supplementary material

Supplementary material is available at *Brain* online.

References

Absinta M, Vuolo L, Rao A, Nair G, Sati P, Cortese IC, et al. Gadolinium-based MRI characterization of leptomeningeal inflammation in multiple sclerosis. Neurology 2015; 85: 18–28.

Agnello D, Carvelli L, Muzio V, Villa P, Bottazzi B, Polentarutti N, et al. Increased peripheral benzodiazepine binding sites and pentraxin 3 expression in the spinal cord during EAE: relation to inflammatory cytokines and modulation by dexamethasone and rolipram. J Neuroimmunol 2000; 109: 105–11.

Arlicot N, Katsifis A, Garreau L, Mattner F, Vergote J, Duval S, et al. Evaluation of CLINDE as potent translocator protein (18 kDa) SPECT radiotracer reflecting the degree of neuroinflammation in a rat model of microglial activation. Eur J Nucl Med Mol Imaging 2008; 35: 2203–11.

Banati RB, Goerres GW, Myers R, Gunn RN, Turkheimer FE, Kreutzberg GW, et al. [11C](R)-PK11195 positron emission tomography imaging of activated microglia in vivo in Rasmussen's encephalitis. Neurology 1999; 53: 2199.

Banati RB, Newcombe J, Gunn RN, Cagnin A, Turkheimer F, Heppner F, et al. The peripheral benzodiazepine binding site in the brain in multiple sclerosis-quantitative in vivo imaging of microglia as a measure of disease activity. Brain 2000; 123: 2321–37.

Beckers L, Ory D, Geric I, Declercq L, Koole M, Kassiou M, et al. Increased expression of translocator protein (TSPO) marks pro-inflammatory microglia but does not predict neurodegeneration. Mol Imaging Biol 2018; 20: 94–102.

Bo L. The histopathology of grey matter demyelination in multiple sclerosis. Acta Neurol Scand Suppl 2009; 120: 51–7.

Bo L, Geurts JJ, Ravid R, Barkhof F. Magnetic resonance imaging as a tool to examine the neuropathology of multiple sclerosis. Neuropathol Appl Neurobiol 2004; 30: 106–17.

Bo L, Vedeler CA, Nyland HI, Trapp BD, Mork SJ. Subpial demyelination in the cerebral cortex of multiple sclerosis patients. J Neuropathol Exp Neurol 2003; 62: 723–32.

Brink BP, Veerhuis R, Breij EC, van der Valk P, Dijkstra CD, Bo L. The pathology of multiple sclerosis is location-dependent: no significant complement activation is detected in purely cortical lesions. J Neuropathol Exp Neurol 2005; 64: 147–55.

Bunai T, Terada T, Kono S, Yokokura M, Yoshikawa E, Futatsubashi M, et al. Neuroinflammation following disease modifying therapy in multiple sclerosis: a pilot positron emission tomography study. J Neurol Sci 2018; 385: 30–3.

Cagnin A, Myers R, Gunn RN, Lawrence AD, Stevens T, Kreutzberg GW, et al. In vivo visualization of activated glia by [11C] (R)-PK11195-PET following herpes encephalitis reveals projected neuronal damage beyond the primary focal lesion. Brain 2001; 124: 2014–27.

Cagnin A, Rossor M, Sampson EL, Mackinnon T, Banati RB. In vivo detection of microglial activation in frontotemporal dementia. Ann Neurol 2004; 56: 894–7.

Chen MK, Guilarte TR. Imaging the peripheral benzodiazepine receptor response in central nervous system demyelination and remyelination. Toxicol Sci 2006; 91: 532–9.

Colasanti A, Guo Q, Muhlert N, Giannetti P, Onega M, Newbould RD, et al. In vivo assessment of brain white matter inflammation in multiple sclerosis with (18)F-PBR111 PET. J Nucl Med 2014; 55: 1112–8.

Cosenza-Nashat M, Zhao ML, Suh HS, Morgan J, Natividad R, Morgello S, et al. Expression of the translocator protein of 18 kDa by microglia, macrophages and astrocytes based on immunohistochemical localization in abnormal human brain. Neuropathol Appl Neurobiol 2009; 35: 306–28.

Datta G, Colasanti A, Kalk N, Owen D, Scott G, Rabiner EA, et al. (11)C-PBR28 and (18)F-PBR111 detect white matter inflammatory heterogeneity in multiple sclerosis. J Nucl Med 2017a; 58: 1477–82.

Datta G, Violante IR, Scott G, Zimmerman K, Santos-Ribeiro A, Rabiner EA, et al. Translocator positron-emission tomography and magnetic resonance spectroscopic imaging of brain glial cell activation in multiple sclerosis. Mult Scler 2017b; 23: 1469–78.

Daugherty DJ, Chechneva O, Mayrhofer F, Deng W. The hGFAP-driven conditional TSPO knockout is protective in a mouse model of multiple sclerosis. Sci Rep 2016; 6: 22556.

Daugherty DJ, Selvaraj V, Chechneva OV, Liu XB, Pleasure DE, Deng W. A TSPO ligand is protective in a mouse model of multiple sclerosis. EMBO Mol Med 2013; 5: 891–903.

De Groot CJ, Bergers E, Kamphorst W, Ravid R, Polman CH, Barkhof F, et al. Post-mortem MRI-guided sampling of multiple sclerosis brain lesions: increased yield of active demyelinating and (p)reactive lesions. Brain 2001; 124: 1635–45.

Debruyne JC, Versijpt J, Van Laere KJ, De Vos F, Keppens J, Strijckmans K, et al. PET visualization of microglia in multiple sclerosis patients using [11C]PK11195. Eur J Neurol 2003; 10: 257–64.

Dickens AM, Vainio S, Marjamaki P, Johansson J, Lehtiniemi P, Rokka J, et al. Detection of microglial activation in an acute model of neuroinflammation using PET and radiotracers 11C-(R)-PK11195 and 18F-GE-180. J Nucl Med 2014; 55: 466–72.

Domene A, Cavanagh C, Page G, Bodard S, Klein C, Delarasse C, et al. Expression of phenotypic astrocyte marker is increased in a transgenic mouse model of Alzheimer's disease versus age-matched controls: a presymptomatic stage study. Int J Alzheimer's Dis 2016; 2016: 5696241.

Edison P, Archer HA, Gerhard A, Hinz R, Pavese N, Turkheimer FE, et al. Microglia, amyloid, and cognition in Alzheimer's disease: an [11C](R)PK11195-PET and [11C]PIB-PET study. Neurobiol Dis 2008; 32: 412–9.

Elliott C, Wolinsky JS, Hauser SL, Kappos L, Barkhof F, Bernasconi C, et al. Slowly expanding/evolving lesions as a magnetic resonance imaging marker of chronic active multiple sclerosis lesions. Mult Scler 2018: 1352458518814117.

Gerhard A, Banati RB, Goerres GB, Cagnin A, Myers R, Gunn RN, et al. [11C](R)-PK11195 PET imaging of microglial activation in multiple system atrophy. Neurology 2003; 61: 686–9.

Gerhard A, Pavese N, Hotton G, Turkheimer F, Es M, Hammers A, et al. In vivo imaging of microglial activation with [11C](R)-PK11195 PET in idiopathic Parkinson's disease. Neurobiol Dis 2006a; 21: 404–12.

Gerhard A, Trender-Gerhard I, Turkheimer F, Quinn NP, Bhatia KP, Brooks DJ. In vivo imaging of microglial activation with [11C](R)-

PK11195 PET in progressive supranuclear palsy. Mov Disord 2006b; 21: 89–93.
Gerhard A, Watts J, Trender-Gerhard I, Turkheimer F, Banati RB, Bhatia K, et al. In vivo imaging of microglial activation with [11C](R)-PK11195 PET in corticobasal degeneration. Mov Disord 2004; 19: 1221–6.
Ghadery C, Koshimori Y, Coakeley S, Harris M, Rusjan P, Kim J, et al. Microglial activation in Parkinson's disease using [(18)F]-FEPPA. J Neuroinflamm 2017; 14: 8.
Giles DA, Washnock-Schmid JM, Duncker PC, Dahlawi S, Ponath G, Pitt D, et al. Myeloid cell plasticity in the evolution of central nervous system autoimmunity. Ann Neurol 2018; 83: 131–41.
Groom GN, Junck L, Foster NL, Frey KA, Kuhl DE. PET of peripheral benzodiazepine binding sites in the microgliosis of Alzheimer's disease. J Nucl Med 1995; 36: 2207–10.
Guilarte TR. TSPO in diverse CNS pathologies and psychiatric disease: a critical review and a way forward. Pharmacol Ther 2019; 194: 44–58.
Harberts E, Datta D, Chen S, Wohler JE, Oh U, Jacobson S. Translocator protein 18 kDa (TSPO) expression in multiple sclerosis patients. J Neuroimmune Pharmacol 2013; 8: 51–7.
Hase Y, Ding R, Harrison G, Hawthorne E, King A, Gettings S, et al. White matter capillaries in vascular and neurodegenerative dementias. Acta Neuropathol Commun 2019; 7: 16.
Hendrickx DAE, van Eden CG, Schuurman KG, Hamann J, Huitinga I. Staining of HLA-DR, Iba1 and CD68 in human microglia reveals partially overlapping expression depending on cellular morphology and pathology. J Neuroimmunol 2017; 309: 12–22.
Henkel K, Karitzky J, Schmid M, Mader I, Glatting G, Unger JW, et al. Imaging of activated microglia with PET and [11C]PK 11195 in corticobasal degeneration. Mov Disord 2004; 19: 817–21.
Herranz E, Gianni C, Louapre C, Treaba CA, Govindarajan ST, Ouellette R, et al. Neuroinflammatory component of gray matter pathology in multiple sclerosis. Ann Neurol 2016; 80: 776–90.
Howell OW, Reeves CA, Nicholas R, Carassiti D, Radotra B, Gentleman SM, et al. Meningeal inflammation is widespread and linked to cortical pathology in multiple sclerosis. Brain 2011; 134: 2755–71.
Israel I, Ohsiek A, Al-Momani E, Albert-Weissenberger C, Stetter C, Mencl S, et al. Combined [18F]DPA-714 micro-positron emission tomography and autoradiography imaging of microglia activation after closed head injury in mice. J Neuroinflamm 2016; 13: 140.
Ji B, Maeda J, Sawada M, Ono M, Okauchi T, Inaji M, et al. Imaging of peripheral benzodiazepine receptor expression as biomarkers of detrimental versus beneficial glial responses in mouse models of Alzheimer's and other CNS pathologies. J Neurosci 2008; 28: 12255–67.
Kaunzner UW, Kang Y, Zhang S, Morris E, Yao Y, Pandya S, et al. Quantitative susceptibility mapping identifies inflammation in a subset of chronic multiple sclerosis lesions. Brain 2019; 142: 133–45.
Kipp M, van der Valk P, Amor S. Pathology of multiple sclerosis. CNS Neurol Disord Drug Targets 2012; 11: 506–17.
Lavisse S, Guillermier M, Herard AS, Petit F, Delahaye M, Van Camp N, et al. Reactive astrocytes overexpress TSPO and are detected by TSPO positron emission tomography imaging. J Neurosci 2012a; 32: 10809–18.
Lavisse S, Guillermier M, Hérard A-S, Petit F, Delahaye M, Van Camp N, et al. Reactive astrocytes overexpress TSPO and are detected by TSPO positron emission tomography imaging. J Neurosci 2012b; 32: 10809–18.
Lavisse S, Inoue K, Jan C, Peyronneau MA, Petit F, Goutal S, et al. [18F]DPA-714 PET imaging of translocator protein TSPO (18 kDa) in the normal and excitotoxically-lesioned nonhuman primate brain. Eur J Nucl Med Mol Imaging 2015; 42: 478–94.
Le Goascogne C, Eychenne B, Tonon MC, Lachapelle F, Baumann N, Robel P. Neurosteroid progesterone is up-regulated in the brain of jimpy and shiverer mice. Glia 2000; 29: 14–24.
Liddelow SA, Guttenplan KA, Clarke LE, Bennett FC, Bohlen CJ, Schirmer L, et al. Neurotoxic reactive astrocytes are induced by activated microglia. Nature 2017; 541: 481–7.
Liu B, Le KX, Park M-A, Wang S, Belanger AP, Dubey S, et al. In vivo detection of age- and disease-related increases in neuroinflammation by 18F-GE180 TSPO micropet imaging in wild-type and Alzheimer's transgenic mice. J Neurosci 2015; 35: 15716–30.
Loth MK, Choi J, McGlothan JL, Pletnikov MV, Pomper MG, Guilarte TR. TSPO in a murine model of Sandhoff disease: presymptomatic marker of neurodegeneration and disease pathophysiology. Neurobiol Dis 2016; 85: 174–86.
Lucchinetti CF, Popescu BF, Bunyan RF, Moll NM, Roemer SF, Lassmann H, et al. Inflammatory cortical demyelination in early multiple sclerosis. N Engl J Med 2011; 365: 2188–97.
Maeda J, Higuchi M, Inaji M, Ji B, Haneda E, Okauchi T, et al. Phase-dependent roles of reactive microglia and astrocytes in nervous system injury as delineated by imaging of peripheral benzodiazepine receptor. Brain Res 2007; 1157: 100–11.
Maeda J, Zhang M-R, Okauchi T, Ji B, Ono M, Hattori S, et al. In Vivo positron emission tomographic imaging of glial responses to amyloid-β and tau pathologies in mouse models of Alzheimer's disease and related disorders. J Neurosci 2011; 31: 4720–30.
Mann DMA, Eaves NR, Marcyniuk B, Yates PO. Quantitative changes in cerebral cortical microvasculature in ageing and dementia. Neurobiol Aging 1986; 7: 321–30.
Martin A, Boisgard R, Theze B, Van Camp N, Kuhnast B, Damont A, et al. Evaluation of the PBR/TSPO radioligand [(18)F]DPA-714 in a rat model of focal cerebral ischemia. J Cereb Blood Flow Metab 2010; 30: 230–41.
Matthews PM, Datta G. Positron-emission tomography molecular imaging of glia and myelin in drug discovery for multiple sclerosis. Expert Opin Drug Discov 2015; 10: 557–70.
Mattner F, Bandin DL, Staykova M, Berghofer P, Gregoire MC, Ballantyne P, et al. Evaluation of [(1)(2)(3)I]-CLINDE as a potent SPECT radiotracer to assess the degree of astroglia activation in cuprizone-induced neuroinflammation. Eur J Nucl Med Mol Imaging 2011; 38: 1516–28.
Meßmer K, Reynolds GP. Increased peripheral benzodiazepine binding sites in the brain of patients with Huntington's disease. Neurosci Lett 1998; 241: 53–6.
Mittelbronn M, Dietz K, Schluesener HJ, Meyermann R. Local distribution of microglia in the normal adult human central nervous system differs by up to one order of magnitude. Acta Neuropathol 2001; 101: 249–55.
Nack A, Brendel M, Nedelcu J, Daerr M, Nyamoya S, Beyer C, et al. Expression of translocator protein and [18F]-GE180 ligand uptake in multiple sclerosis animal models. Cells 2019; 8: 94.
Narayan N, Mandhair H, Smyth E, Dakin SG, Kiriakidis S, Wells L, et al. The macrophage marker translocator protein (TSPO) is down-regulated on pro-inflammatory 'M1' human macrophages. PLoS One 2017; 12: e0185767.
Nguyen DL, Wimberley C, Truillet C, Jego B, Caille F, Pottier G, et al. Longitudinal positron emission tomography imaging of glial cell activation in a mouse model of mesial temporal lobe epilepsy: toward identification of optimal treatment windows. Epilepsia 2018; 59: 1234–44.
Oh U, Fujita M, Ikonomidou VN, Evangelou IE, Matsuura E, Harberts E, et al. Translocator protein PET imaging for glial activation in multiple sclerosis. J Neuroimmune Pharmacol 2011; 6: 354–61.
Okello A, Edison P, Archer HA, Turkheimer FE, Kennedy J, Bullock R, et al. Microglial activation and amyloid deposition in mild cognitive impairment: a PET study. Neurology 2009; 72: 56–62.
Ouchi Y, Yoshikawa E, Sekine Y, Futatsubashi M, Kanno T, Ogusu T, et al. Microglial activation and dopamine terminal loss in early Parkinson's disease. Ann Neurol 2005; 57: 168–75.

Owen DR, Narayan N, Wells L, Healy L, Smyth E, Rabiner EA, et al. Pro-inflammatory activation of primary microglia and macrophages increases 18 kDa translocator protein expression in rodents but not humans. J Cereb Blood Flow Metab 2017; 37: 2679–90.

Peferoen LA, Vogel DY, Ummenthum K, Breur M, Heijnen PD, Gerritsen WH, et al. Activation status of human microglia is dependent on lesion formation stage and remyelination in multiple sclerosis. J Neuropathol Exp Neurol 2015; 74: 48–63.

Politis M, Giannetti P, Su P, Turkheimer F, Keihaninejad S, Wu K, et al. Increased PK11195 PET binding in the cortex of patients with MS correlates with disability. Neurology 2012; 79: 523–30.

Politis M, Lahiri N, Niccolini F, Su P, Wu K, Giannetti P, et al. Increased central microglial activation associated with peripheral cytokine levels in premanifest Huntington's disease gene carriers. Neurobiol Dis 2015; 83: 115–21.

Ratchford JN, Endres CJ, Hammoud DA, Pomper MG, Shiee N, McGready J, et al. Decreased microglial activation in MS patients treated with glatiramer acetate. J Neurol 2012; 259: 1199–205.

Ravikumar B, Crawford D, Dellovade T, Savinainen A, Graham D, Liere P, et al. Differential efficacy of the TSPO ligands etifoxine and XBD-173 in two rodent models of Multiple Sclerosis. Neuropharmacology 2016; 108: 229–37.

Rissanen E, Tuisku J, Rokka J, Paavilainen T, Parkkola R, Rinne JO, et al. In vivo detection of diffuse inflammation in secondary progressive multiple sclerosis using PET imaging and the radioligand (1)(1)C-PK11195. J Nucl Med 2014; 55: 939–44.

Rojas S, Martín A, Arranz MJ, Pareto D, Purroy J, Verdaguer E, et al. Imaging brain inflammation with [11C]PK11195 by PET and induction of the peripheral-type benzodiazepine receptor after transient focal ischemia in rats. J Cereb Blood Flow Metab 2007; 27: 1975–86.

Ryu JK, Choi HB, McLarnon JG. Peripheral benzodiazepine receptor ligand PK11195 reduces microglial activation and neuronal death in quinolinic acid-injected rat striatum. Neurobiol Dis 2005; 20: 550–61.

Sethi V, Nair G, Absinta M, Sati P, Venkataraman A, Ohayon J, et al. Slowly eroding lesions in multiple sclerosis. Mult Scler 2017; 23: 464–72.

Sucksdorff M, Rissanen E, Tuisku J, Nuutinen S, Paavilainen T, Rokka J, et al. Evaluation of the effect of fingolimod treatment on microglial activation using serial PET imaging in multiple sclerosis. J Nucl Med 2017; 58: 1646–51.

Sérrière S, Tauber C, Vercouillie J, Mothes C, Pruckner C, Guilloteau D, et al. Amyloid load and translocator protein 18 kDa in APPswePS1-dE9 mice: a longitudinal study. Neurobiol Aging 2015; 36: 1639–52.

Tai YF, Pavese N, Gerhard A, Tabrizi SJ, Barker RA, Brooks DJ, et al. Imaging microglial activation in Huntington's disease. Brain Res Bull 2007; 72: 148–51.

Tomasi G, Edison P, Bertoldo A, Roncaroli F, Singh P, Gerhard A, et al. Novel reference region model reveals increased microglial and reduced vascular binding of 11C-(R)-PK11195 in patients with Alzheimer's disease. J Nucl Med 2008; 49: 1249–56.

Turner MR, Cagnin A, Turkheimer FE, Miller CC, Shaw CE, Brooks DJ, et al. Evidence of widespread cerebral microglial activation in amyotrophic lateral sclerosis: an [11C](R)-PK11195 positron emission tomography study. Neurobiol Dis 2004a; 15: 601–9.

Turner MR, Cagnin A, Turkheimer FE, Miller CCJ, Shaw CE, Brooks DJ, et al. Evidence of widespread cerebral microglial activation in amyotrophic lateral sclerosis: an [11C](R)-PK11195 positron emission tomography study. Neurobiol Dis 2004b; 15: 601–9.

van der Knaap MS, Bugiani M. Leukodystrophies: a proposed classification system based on pathological changes and pathogenetic mechanisms. Acta Neuropathol 2017; 134: 351–82.

van der Valk P, De Groot CJ. Staging of multiple sclerosis (MS) lesions: pathology of the time frame of MS. Neuropathol Appl Neurobiol 2000; 26: 2–10.

van Horssen J, Brink BP, de Vries HE, van der Valk P, Bo L. The blood-brain barrier in cortical multiple sclerosis lesions. J Neuropathol Exp Neurol 2007; 66: 321–8.

Veiga S, Azcoitia I, Garcia-Segura LM. Ro5-4864, a peripheral benzodiazepine receptor ligand, reduces reactive gliosis and protects hippocampal hilar neurons from kainic acid excitotoxicity. J Neurosci Res 2005; 80: 129–37.

Venneti S, Lopresti BJ, Wang G, Hamilton RL, Mathis CA, Klunk WE, et al. PK11195 labels activated microglia in Alzheimer's disease and in vivo in a mouse model using PET. Neurobiol Aging 2009; 30: 1217–26.

Venneti S, Lopresti BJ, Wiley CA. The peripheral benzodiazepine receptor (translocator protein 18kDa) in microglia: from pathology to imaging. Prog Neurobiol 2006; 80: 308–22.

Veronese M, Reis Marques T, Bloomfield PS, Rizzo G, Singh N, Jones D, et al. Kinetic modelling of [11C]PBR28 for 18 kDa translocator protein PET data: a validation study of vascular modelling in the brain using XBD173 and tissue analysis. J Cereb Blood Flow Metab 2018; 38: 1227–42.

Versijpt J, Debruyne JC, Van Laere KJ, De Vos F, Keppens J, Strijckmans K, et al. Microglial imaging with positron emission tomography and atrophy measurements with magnetic resonance imaging in multiple sclerosis: a correlative study. Mult Scler 2005; 11: 127–34.

Vogel DY, Vereyken EJ, Glim JE, Heijnen PD, Moeton M, van der Valk P, et al. Macrophages in inflammatory multiple sclerosis lesions have an intermediate activation status. J Neuroinflamm 2013; 10: 35.

Vowinckel E, Reutens D, Becher B, Verge G, Evans A, Owens T, et al. PK11195 binding to the peripheral benzodiazepine receptor as a marker of microglia activation in multiple sclerosis and experimental autoimmune encephalomyelitis. J Neurosci Res 1997; 50: 345–53.

Wang Y, Yue X, Kiesewetter DO, Niu G, Teng G, Chen X. PET imaging of neuroinflammation in a rat traumatic brain injury model with radiolabeled TSPO ligand DPA-714. Eur J Nucl Med Mol Imaging 2014; 41: 1440–9.

Wimberley C, Lavisse S, Brulon V, Peyronneau MA, Leroy C, Bodini B, et al. Impact of endothelial 18-kDa translocator protein on the quantification of (18)F-DPA-714. J Nucl Med 2018; 59: 307–14.

Yankam Njiwa J, Costes N, Bouillot C, Bouvard S, Fieux S, Becker G, et al. Quantitative longitudinal imaging of activated microglia as a marker of inflammation in the pilocarpine rat model of epilepsy using [11C]-(R)-PK11195 PET and MRI. J Cereb Blood Flow Metab 2017; 37: 1251–63.

Yasuno F, Ota M, Kosaka J, Ito H, Higuchi M, Doronbekov TK, et al. Increased binding of peripheral benzodiazepine receptor in Alzheimer's disease measured by positron emission tomography with [11C]DAA1106. Biol Psychiatry 2008; 64: 835–41.

Zrzavy T, Hametner S, Wimmer I, Butovsky O, Weiner HL, Lassmann H. Loss of 'homeostatic' microglia and patterns of their activation in active multiple sclerosis. Brain 2017; 140: 1900–13.